INTERNATIONAL JOURNAL FOR NUMERICAL METHODS IN FLUIDS, VOL. 23, 1241–1262 (1996)

CALCULATION OF STEADY AND OSCILLATING FLOWS IN TUBES USING A VORTICITY TRANSPORT ALGORITHM

A. W. JOHNSON AND J. H. GERRARD

The Manchester School of Engineering, University of Manchester, Manchester M13 9PL, U.K.

SUMMARY

Steady and oscillating axisymmetric tube flows are modelled using a vorticity transport algorithm. The axisymmetric convective–diffusive Navier–Stokes equations are solved using a splitting technique. Axisymmetric ring vortex filaments are introduced on the walls and subsequently convected and diffused throughout the flow field. An axisymmetric equation similar to the Oseen diffusion equation is used to diffuse the ring vortex filaments. Vorticity is reflected from the tube walls using two techniques. Results are presented for the developing Poiseuille flow and for the developed flow in the form of the entrance length and the axial velocity and vorticity profiles. Good agreement is achieved with a finite difference method in the developing region of Poiseuille flow. The developed flow results are compared with the analytical solutions. The developed profiles of velocity and vorticity have errors of less than 0·3 per cent for both methods of dealing with reflection of diffusion at the bounding surfaces and similar accuracy is obtained for the velocity profiles in oscillating flow except at the wall. Oscillating flow is produced with a discretized sinusoidal piston motion. Velocity profiles, boundary layer thickness and entrance length are presented for oscillating flow. Good agreement is achieved for low-Womersley-number non-dimensional frequency. At higher values of this parameter, flows are inaccurately simulated, because the number of piston positions used to discretize the piston motion is inversely proportional to the non-dimensional frequency.

KEY WORDS: axisymmetric flow; vortex method; laminar flow; entrance length; steady and oscillating flows

1. INTRODUCTION

The extension of Lagrangian vortex element methods to the computation of unsteady viscous flows from two to three dimensions has evolved in recent years.[1,2] A description of a two-dimensional computational model which was applied to the flow past a circular cylinder has been published by Benson *et al.*[3] and is the basis of the present work. For axisymmetric flows the non-dimensional convective–diffusive Navier–Stokes equations are solved by the introduction of ring vortex filaments to represent a shear layer on the solid surfaces and by the subsequent convection and diffusion of these vortex filaments. The convection routine involves a cloud- in-cell type of calculation as given by Christiansen[4] and the diffusion routine involves the redistribution of circulation on a mesh. The diffusion is computed from the axisymmetric solution which is derived in the Appendix. To ensure the conservation of vorticity near the solid surfaces, vorticity must be 'treated' in these regions. Two approximate methods of wall treatment are compared: vorticity is either specularly reflected from the solid surfaces or is allowed to diffuse beyond the solid surfaces, reallocated to mesh points and rediffused into the flow field. Results are presented using both methods. The flows are produced by the motion of a piston. Wagner[5] discusses the difficulties associated with specification of the inlet

CCC 0271–2091/96/121241–22

Received August 1995
Revised February 1996

conditions when a piston is not employed. The Poiseuille flow results are shown in the form of the developed velocity and vorticity profiles, whilst the oscillating flow results are in the form of the developed velocity profiles only. The performance of the computational scheme is tested by comparison with analytical solutions[6,7] for steady and oscillating flows started from rest in a tube of circular cross-section. The developing steady flow is shown to agree with a finite difference solution of Friedman *et al.*[8] and experimental results quoted by Schlichting.[9]

2. VORTICITY TRANSPORT ALGORITHM

For both the developing Poiseuille and oscillating flow situations, axisymmetric cylindrical co-ordinates (r, z) are introduced, where r is the radial co-ordinate and z is the axial co-ordinate. The origin is at the entrance to the tube.

The non-dimensional axisymmetric Navier–Stokes equations in vorticity– streamfunction form are

$$\frac{\partial \eta}{\partial t} = -\frac{\partial (u\eta)}{\partial z} - \frac{\partial (v\eta)}{\partial r} + \frac{1}{Re}\left(\frac{\partial^2 \eta}{\partial z^2} + \frac{\partial^2 \eta}{\partial r^2} + \frac{1}{r}\frac{\partial \eta}{\partial r} - \frac{\eta}{r^2}\right) \tag{1}$$

and the azimuthal component of vorticity in axisymmetric co-ordinates satisfies the equation

$$\frac{1}{r}\left(\frac{\partial^2 \psi}{\partial z^2} + \frac{\partial^2 \psi}{\partial r^2} - \frac{1}{r}\frac{\partial \psi}{\partial r}\right) = -\eta, \tag{2}$$

where η is the vorticity, ψ is the Stokes streamfunction, u is the axial velocity, v is the radial velocity and Re is the characteristic flow Reynolds number based on the tube radius and the cross- sectional mean velocity which, when the flow is driven by a piston, is the piston velocity. In oscillating flow the maximum piston velocity is used.

In axisymmetric co-ordinates the velocity components are related to the Stokes streamfunction by

$$u = \frac{1}{r}\frac{\partial \psi}{\partial r}, \tag{3}$$

$$v = -\frac{1}{r}\frac{\partial \psi}{\partial z}. \tag{4}$$

To solve these equations, an algorithm is adopted and developed which assumes that the convective and diffusive vorticity transport processes can be split and treated separately.[3,10]

In the present flow situations, flow starts from rest at $t = 0$. To satisfy the no-slip condition, vorticity is introduced at the tube wall from where it diffuses into the fluid. Vorticity is represented by discrete ring vortex filaments. These are convected using the cloud-in-cell method of Christiansen.[4] Vorticity is diffused using a relationship equivalent to the Oseen equation for two-dimensional flow. After diffusion has occurred, vorticity is redistributed into new ring vortex filaments of zero age located at the mesh points. For convectional accuracy purposes the cloud-in-cell method is applied several times between each circulation redistribution step. The relative rates of calling are controlled by the following time steps:

$$DTR = NRAT1 \cdot DTT,$$

where DTT is the convection time step and DTR is the diffusion time step.

The no-slip condition is satisfied by the introduction of a vortex sheet on the solid surfaces. This sheet is discretized into ring vortex filaments of a strength equal to the negative tangential wall velocity multiplied by the mesh length. Surface vorticity is only created in the convection routine

prior to each redistribution step, because its effect in satisfying the no-slip condition is not apparent until vorticity diffuses away from the solid surfaces.

The detail of the sequence of events in the basic time step *DTR* was originally as follows.

(i) Elementary ring vortices are introduced at the mesh points on the boundaries to satisfy the no-slip condition and are given the vortex age *DTR*. Previously introduced vortices at this time have the same age but are not on mesh points, having been convected *NRAT*1 times during the previous time step.

(ii) All vortices are diffused onto surrounding mesh intersections. At the end of the diffusion step, new vortices are created at the mesh points and have zero age attributed to them.

(iii) After one convection time step *DTT* the velocities at the mesh intersections are determined by finite difference calculation from the streamfunction values obtained as described in the next section. Vortices are convected distances derived from these velocities acting for a time *DTT* and their positions stored. The new vortices are inserted after the scan of the whole field. The convection process is repeated *NRAT*1 times and the end of the diffusion step reached after the time *DTR*.

In the Appendix, vortices are diffused from grid points to ease the calculation on a hand calculator. In general the vortices are not on grid points but are diffused to grid points. Each contribution to the grid point is added to what is there already. Once diffusion takes place, the vortex strength of the diffusing vortex has dropped to zero and is not included in the vorticity field after diffusion.

The original method of diffusion was superseded by the symmetrical method which was used throughout. This method can be employed when the mesh is uniform in the z-direction. If *DZD* is the z-direction mesh interval and n is an integer, diffusion from the mesh point r, z transfers the same vortex strength to the mesh points $r_1, z - n \cdot DZD$ and $r_1, z + n \cdot DZD$. We therefore first place the vortices on the mesh points by an area-weighting scheme. The vorticity distribution remains essentially the same. Making use of this symmetry reduced the number of individual diffusion calculations by almost a half.

3. CONVECTION ROUTINE

The routine used to convect the vortices is similar to that used by Benson *et al.*[3] This routine is employed to solve the convection part of equation (1), i.e.

$$\frac{\partial \eta}{\partial t} = -\frac{\partial (u\eta)}{\partial z} - \frac{\partial (v\eta)}{\partial r}.$$

The velocities of the vortices are calculated using the cloud-in-cell method. The cloud-in-cell method involves the discretization of the circulation onto the grid points using an area-weighting scheme. The streamfunction distribution is subsequently obtained from the vorticity distribution by solving equation (2). The velocities at the vortex locations are calculated and the vortices are convected with these velocities.

To solve an axisymmetric partial differential equation to obtain the streamfunction ψ from the known source function η, the NAG fortran library routines D03EDF and D03EEF were used. These solve seven-diagonal systems of linear equations which arise from the discretization of an elliptic partial differential equation on a rectangular region using a multigrid technique. The solver imposes a restriction that both the axial and radial mesh point numbers are of the form $2^n + 1$, where n is an integer, and thus optimized routine convergence is achieved. The solver required the specification of the streamfunction on the boundaries of the computational region. The boundary conditions are as follows.

(a) At the inlet to the flow region for $t \geqslant 0$, $u = U_0$ and $v = 0$. The streamfunction is obtained by integrating equation (3). The boundary condition is

$$\psi_{\text{inlet}} = U_0 r^2/2.$$

(b) It follows from axisymmetry that $v = 0$ on the centreline and thus ψ is a constant which is put equal to zero,

$$\psi_{\text{cl}} = 0.$$

(c) The streamfunction boundary condition at the wall is equal to a constant which is obtained from equation (3) and

$$\psi_{\text{wall}} = U_0 r_{\text{wall}}^2/2.$$

(d) The condition imposed in the current model in order to obtain the downstream boundary condition is $v = 0$. This implies the Neumann condition

$$\partial\psi/\partial z = 0$$

at the downstream boundary.

On completion of the streamfunction calculations it is necessary to obtain the axial velocity u and radial velocity v. Equations (3) and (4) are evaluated using central finite differences to calculate the internal velocity field. At the wall and centreline a higher-order expression is used to calculate the axial velocities. At the centreline and wall the radial velocity is equal to zero.

4. DIFFUSION ROUTINE

The diffusion equation to be solved is

$$\frac{\partial\eta}{\partial t} = \frac{1}{Re}\left(\frac{\partial^2\eta}{\partial z^2} + \frac{\partial^2\eta}{\partial r^2} + \frac{1}{r}\frac{\partial\eta}{\partial r} - \frac{\eta}{r^2}\right).$$

The solution involves the diffusion of vorticity to the surrounding mesh points for a time equal to the diffusion time step. Following this reallocation, vortices of zero age are created at the mesh points. An equation for the diffusion of a vortex ring is derived in the Appendix. The vorticity diffused from a ring vortex filament with radius r' to a point at radius r is given by

$$\eta = \eta_{\text{os}}\pi^{1/2}\frac{r'}{\sqrt{(vt)}}e^{-rr'/2vt}I_1\left(\frac{rr'}{2vt}\right),$$

where n_{os} is the value of the Oseen vorticity expression at point P, I_1 is the modified Bessel function of the first kind of order one and t is the age of the vortex.

The choice of time step is determined by the requirement that it be small enough to produce a faithful representation of the actual continuous variation. The diffusion time step must be large enough to produce a spread of vorticity and is therefore larger than the convection time step. In two-dimensional flow the conservation of circulation in the diffusion step can be checked and a small correction applied to ensure exact conservation. In the present axisymmetric flow, vorticity is zero on the axis and circulation is lost by overlapping of circulation from opposite sides of the vortex ring element (see Appendix). The maximum number of mesh lengths, *KTOL*, from the diffusing ring for which diffusion is calculated must be large enough to automatically conserve circulation in the body of the flow whilst allowing circulation to be lost near the axis. If *KTOL* is larger than necessary,

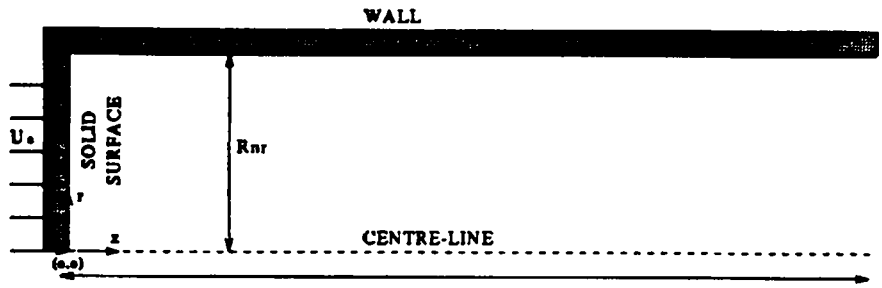

Figure 1(a). Developing Poiseuille flow computational region

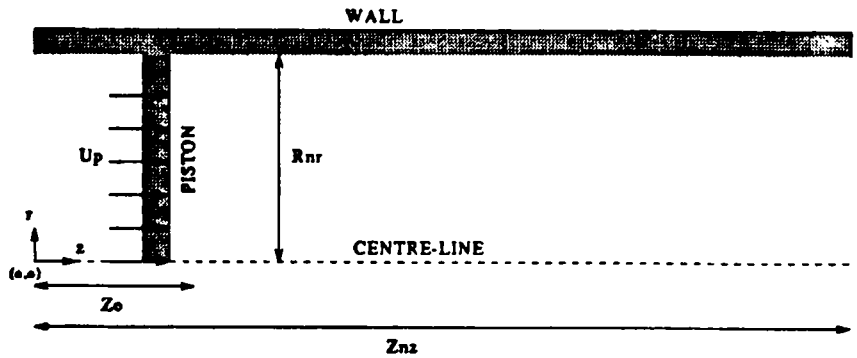

Figure 1(b). Oscillating flow computational region

computing time is wasted in redistributing negligible vorticity. Generally *KTOL* only needed to be one greater than the two-dimensional value.

In the original method of calculating diffusion (inherited from the two- dimensional model of Benson *et al.*[3]), vorticity was diffused to the surrounding mesh points from vortices which were not on mesh points. Considerable computing time was saved by placing the vortices on mesh points by an area-weighting scheme and making use of symmetry of diffusion in the z-direction, $\eta(r, z + \delta z) = \eta(r, z - \delta z)$. This method did not affect the accuracy and was employed throughout.

The tube flows under investigation involve the diffusion of vorticity beyond the flow boundaries. At the downstream boundary there is assumed to be no vorticity variation with downstream length. The regions of particular interest are the solid boundaries. Benson *et al.*[3] in two dimensions effectively use a specular reflection to account for this diffusion. Two methods have been investigated during the current axisymmetric work. The first is a specular reflection similar to that used by Benson *et al.*[3] The second is a method by which vorticity is allowed to diffuse beyond the solid boundaries, reallocated to mesh points and rediffused into the flow field for a time equal to the age of the original vortex. We have called this method an extraneous diffusion technique.

Specular reflection implies that the effect of the wall is assumed to reflect the diffusion back into the flow in the plane of the flow in Figures 1(a) and 1(b) in a two-dimensional fashion. It is clear from

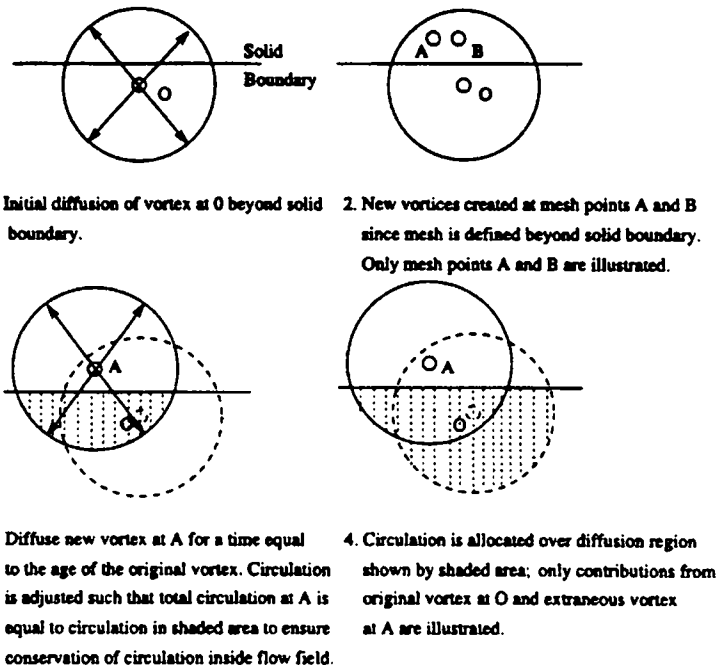

1. Initial diffusion of vortex at 0 beyond solid boundary.
2. New vortices created at mesh points A and B since mesh is defined beyond solid boundary. Only mesh points A and B are illustrated.
3. Diffuse new vortex at A for a time equal to the age of the original vortex. Circulation is adjusted such that total circulation at A is equal to circulation in shaded area to ensure conservation of circulation inside flow field.
4. Circulation is allocated over diffusion region shown by shaded area; only contributions from original vortex at O and extraneous vortex at A are illustrated.

Figure 2. Extraneous diffusion method

Figure 17 in the Appendix that diffusion is not restricted to this plane. Some error is introduced near the wall as will be shown in Section 7 and Figures 3–5. The errors are reduced by the use of extraneous diffusion at the expense of computing time.

In both methods the uniform mesh is extended beyond the walls. In specular reflection the vortex strength diffused to a grid point at n mesh lengths outside the wall is placed at the same z-position at n mesh lengths on the interior side of the wall. Circulation is thus automatically conserved. The method of extraneous diffusion is described in Figure 2.

5. DEVELOPING POISEUILLE FLOW

The vorticity transport algorithm has been adapted to model the development of a flow from the entrance of a rigid tube where the velocity is uniform over the cross-section to the Poiseuille flow velocity distribution at the end of the entrance length. The flow region is as shown in Figure 1(a). This figure shows that an impulsively started solid surface moving with a uniform velocity U_0 has been introduced at the tube entrance where $z=0$. The solid surface remains at $z=0$, i.e. the origin moves with the piston. A solid piston has the advantage that the tube entry is precisely specified. No-slip vortices are introduced on the piston surface and diffusion which would cross the piston is dealt with by the reflection method in use. The flow in front of the piston is developing Poiseuille flow.

The non-dimensional parameter used in equation (1) is the characteristic flow Reynolds number based on the tube radius,

$$Re_r = U_0 r_{\text{tube}}/\nu,$$

where U_0 is the velocity at the tube entrance, Re_r and Re_d specify Reynolds numbers based on tube radius and diameter respectively.

The mesh used to model the flow region is a simple rectangular mesh of axial and radial spacings *DZD* and *DRD* respectively and numbers of axial and radial mesh points *NZ* and *NR* respectively. The following parameters have been used as input to the Poiseuille flow model: $U_0 = 1{\cdot}0$, $R_{NR} = 1{\cdot}0$, $NR = 33$, $Z_{NZ} = 16{\cdot}0$, $NZ = 513$, $NRAT1 = 3$, $KTOL = 4$.

6. OSCILLATING FLOW PRODUCED BY A RECIPROCATING PISTON IN A RIGID TUBE

The adaption of the vorticity transport algorithm to the oscillating flow situation is somewhat more complicated than the steady flow application. The model described here involves the discretization of a sinusoidal piston motion into a series of piston steps. The following equation describes the sinusoidal piston motion:

$$Z_p = Z_0[1 - \cos(\omega t)], \tag{5}$$

where Z_p is the piston position at time t, Z_0 is the piston amplitude and ω is the angular frequency of the piston. Initially the piston is given an impulsive start from its rest position where $t = 0$. At each piston step the vorticity transport algorithm is employed to calculate the flow field. The flow field is calculated for a time equal to the piston time step. The piston is subsequently moved to its next step position and the flow field calculation is repeated. Since the fluid under consideration is assumed to be incompressible, when the piston is moved, the vortices produced during the flow calculation are moved axially by the same amount.

The flow field under consideration is illustrated by Figure 1(b). The 'inlet' or piston surface moves relative to the origin. As in the developing Poiseuille flow model, a simple rectangular mesh is used to define the flow region. The axial mesh is defined relative to this surface and moves with the piston. This involves the definition of a new axial grid at each piston step. The radial mesh used is identical with that used by the Poiseuille flow model.

The non-dimensional parameter used in equation (1) to represent the oscillating flow is the Reynolds number based on the maximum piston velocity,

$$Re_r = U_p r_{tube}/\nu. \tag{6}$$

In an oscillating flow the Reynolds number is not the only relevant non- dimensional parameter. The dominant parameter used as an input to this model is the Womersley parameter α, where

$$\alpha = r_{tube}(\omega/\nu)^{1/2}. \tag{7}$$

The Womersley parameter is equal to the ratio of the tube radius to the distance from the wall over which vorticity diffuses in one piston oscillation. Combining equations (6) and (7) gives

$$Re = U_p \alpha^2/\omega r_{tube}.$$

In addition to the counter *NRAT*1 (the number of convection steps per diffusion step), further counters must be introduced to model an oscillating flow. A counter *NRAT2* is used to represent the number of diffusion steps per piston step. *NCT* is the number of convection steps per piston time step and is defined as

$$NCT = NRAT1 \cdot NRAT2.$$

The following parameters are used as input to the oscillating flow model: $\nu = 0{\cdot}01$, $R_{NR} = 1{\cdot}0$, $NR = 33$, $Z_{NZ} = 8{\cdot}0$, $NZ = 257$, $Z_0 = 0{\cdot}25$, $NRAT1 = 3$, $NRAT2 = 2$, $KTOL = 3$.

6.1. *Calculation of reciprocating piston parameters*

The initial calculations made by this model are those of the piston parameters, i.e. the axial piston position, the piston velocity and the piston time step. Using equation (7), the angular frequency ω may be calculated. Defining the period in terms of the number of piston steps, *NZP*, the number of convection time steps per piston time step, *NCT*, and the convection time step *DTT* enables the calculation of the number of piston positions as

$$NZP = \frac{\pi}{\omega \cdot NCT \cdot DTT} + 1.$$

The sinusoidal piston motion is given by equation (5). This motion may be defined in terms of *NZP* as

$$Z_p(I) = Z_0\left[1 - \cos\left(\frac{\pi(I-1)}{NZP-1}\right)\right],$$

where $Z_p(I)$ is the axial piston position at piston position I. The piston axial velocities are subsequently determined using a central finite difference expression for

$$U_p = \partial Z_p / \partial t.$$

Note that the piston time step is constant whilst the piston velocity and the axial piston position vary sinusoidally.

7. RESULTS AND DISCUSSION

The Poiseuille flow developed axial velocity and vorticity profiles are respectively parabolic and linear. The departure from these curves is shown in Figures 3 and 4 for the specular reflection and extraneous diffusion cases respectively. The developed axial velocity profile does not vary significantly with time. The developed vorticity profile varies with time only at the wall. Figures 3 and 4 illustrate instantaneous profiles. Both methods give results which are in good agreement with the exact solutions. The extraneous diffusion method gives more accurate results near the tube wall. This is shown by Figure 5 for the same Reynolds number, which illustrates the downstream developed wall vorticity variation with time. The developed wall vorticity varies with time owing to the convection, diffusion and no-slip introduction processes. The exact value of the developed wall vorticity is 4·0. The wall vorticity values obtained using the specular reflection method vary about a central value of 4·0729, whilst the more accurate extraneous diffusion method gives a central value of 4·0008. However, the more accurate extraneous diffusion method is computationally intensive compared with the specular reflection case. For example, an extraneous diffusion computational run to a time at which the downstream centreline velocity is 99 per cent of its fully developed value, using a Reynolds number of 40 based on diameter, $Z_{NZ} = 8{\cdot}0$ and $NZ = 257$, has a CPU run time on an HP710 workstation of 11,401 s, whilst the corresponding specular reflection case has a CPU run time of 3186 s.

Figure 6 shows the axial velocity development downstream at various radial positions for a Reynolds number of 40 (based on diameter to enable comparison with previously published results). The overshoot phenomenon, i.e. the peak in axial velocity near the tube wall and near the tube entrance, proved theoretically to exist by Benson and Trogden,[11] can be clearly seen. The apparent peak in axial velocity on the tube wall and near the tube entrance is due to a singularity at the tube entrance and on the tube wall. Here the specification of the inlet axial velocity is difficult owing to the physical discontinuity in axial velocity at the corner; a velocity of 0·0 was used. Good agreement is achieved with the results of Friedmann *et al.*[8] for the development of centreline axial velocity at a

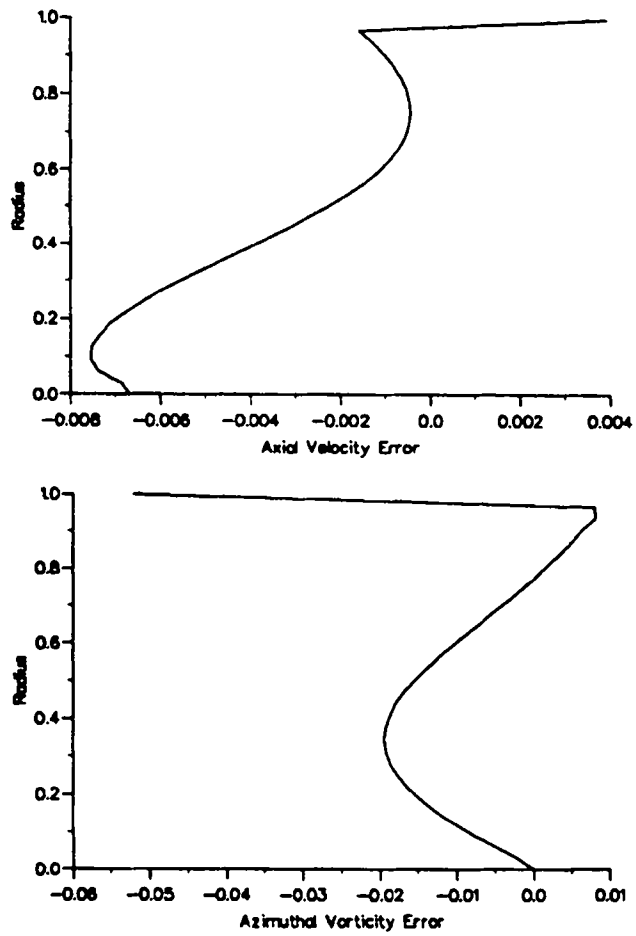

Figure 3. Poiseuille flow developed velocity and vorticity errors obtained using specular reflection method with exact solutions. Full line denotes present results ($Re_d = 40$)

Reynolds number of 40. The entrance length values obtained using this method are similar to those given by previous authors as seen in Table I. Atabek *et al.*[12] noted the uncertainty in determining the position of the tube entrance when using an experimental technique and calculated a small correction using a combined theoretical and experimental method. This correction amounted to 1·5 per cent of the entrance length. Both the specular reflection and extraneous diffusion methods give

Table I. Poiseuille flow entrance length comparison

	Entrance length		
Re	Present results	Friedmann *et al.*[8]	Schlichting[9]
40	4·875	4·9	4·6
100	11·5	11·3	11·5

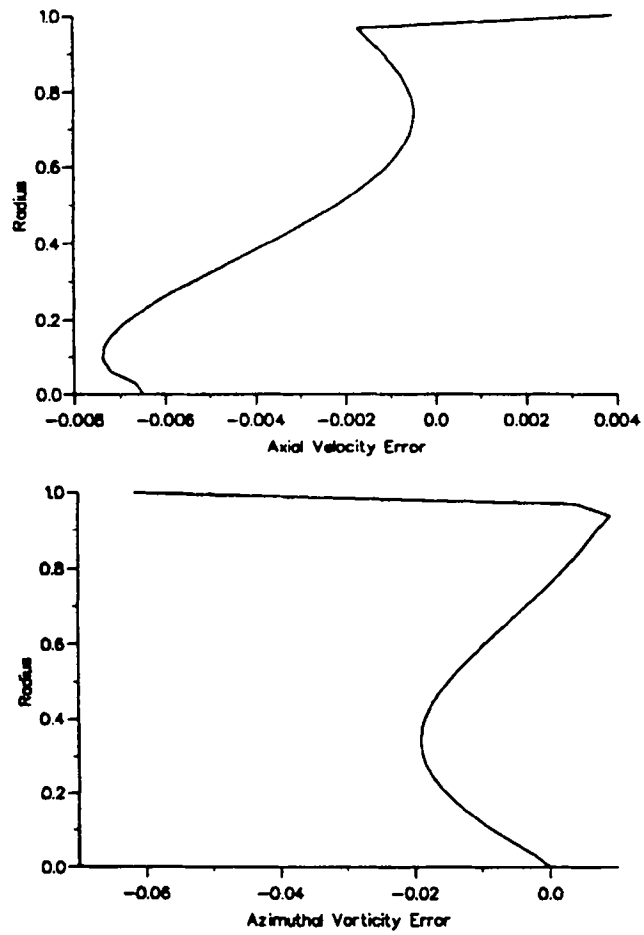

Figure 4. Poiseuille flow developed velocity and vorticity errors obtained using extraneous diffusion method with exact solutions. Full line denotes present results ($Re_d = 40$)

approximately the same result for entrance length. The Schlichting values are the result of his appraisal of experimental values.

The oscillating flow results are presented at two times during a piston oscillation: at the end of a piston oscillation where $\theta = 2\pi$ and the cross-sectional mean velocity equals zero and at the maximum reverse piston velocity where $\theta = 3\pi/2$. The developed axial velocity profiles at the above times are presented in Figures 7 and 8 for the specular reflection and extraneous diffusion techniques respectively for a range of Womersley α-values. The deviation of these results from the analytical solution of Womersley[6] is presented in Figures 9 and 10 respectively. At a low Womersley number, e.g. $\alpha = 2{\cdot}5$, it appears that both the extraneous diffusion and specular reflection methods give accurate solutions. However, at a high Womersley number, e.g. $\alpha = 25{\cdot}0$, both methods give erroneous results. There is a lower developed axial velocity error near the wall at the maximum reverse piston velocity than at the end of a piston oscillation. The error in axial velocity varies with time. The error variation is periodic in the developed oscillating flow and is illustrated by Figure 11 for a Womersley number of 3·5 using the specular reflection method. The lower figure of Figure 11 is a magnification of the top figure at later times when the fully developed oscillating flow has been

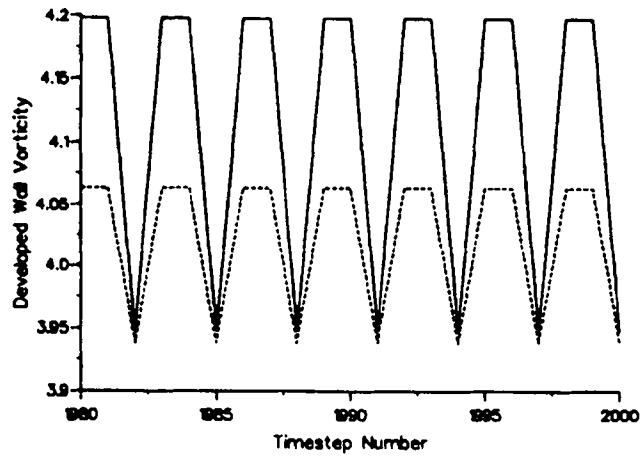

Figure 5. Comparison of developed wall vorticity using different wall treatment methods at $Re_d = 40$. Full line denotes specular reflection. Broken line denotes extraneous diffusion

achieved. The axial velocity error varies sinusoidally with time near the tube wall and varies with a wave-form possessing distinctive peaks near the centreline. Note that the errors are of a small magnitude and the large errors at small times are due to the invalidity of the analytical solution when the developed oscillating flow situation has not been achieved.

The increasing error with Womersley number is shown by Figures 9 and 10. The reason for this increasing error is the low number of piston positions, *NZP*, used at higher Womersley numbers. For example, using the input parameters previously defined, a Womersley number of 25·0 results in only nine piston positions, whilst a Womersley number of 3·5 results in 407 piston positions. The discretization of the sinusoidal piston motion is more accurately performed at low Womersley numbers. For a particular Womersley number the number of piston positions, *NZP*, is dependent on the value of mesh length, which is a minimum due to computational restrictions, *KTOL*, the number of mesh lengths over which vorticity can diffuse in a single diffusion step, and *NRAT*2, the number of diffusion steps per piston step. *NRAT*2 is greater than or equal to one, since diffusion must occur on

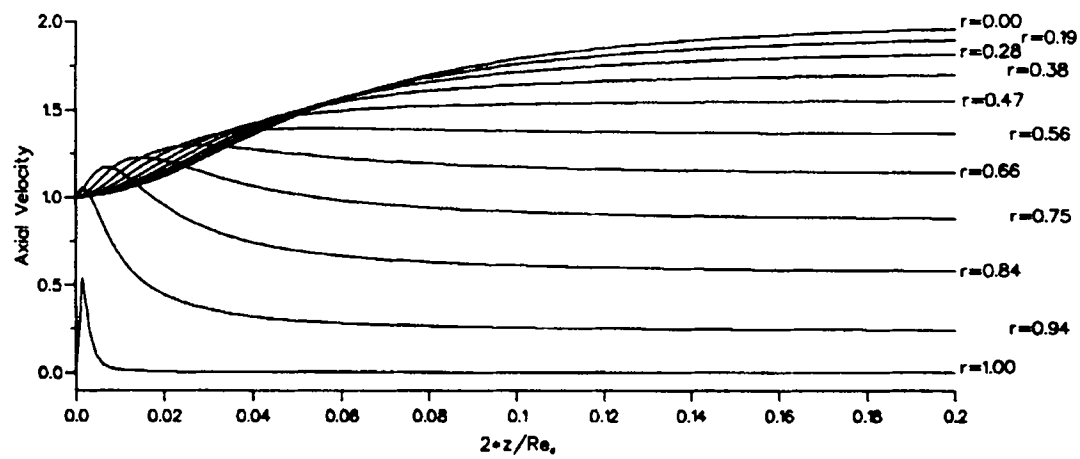

Figure 6. Axial velocity downstream development for Poiseuille flow, $Re_d = 40$

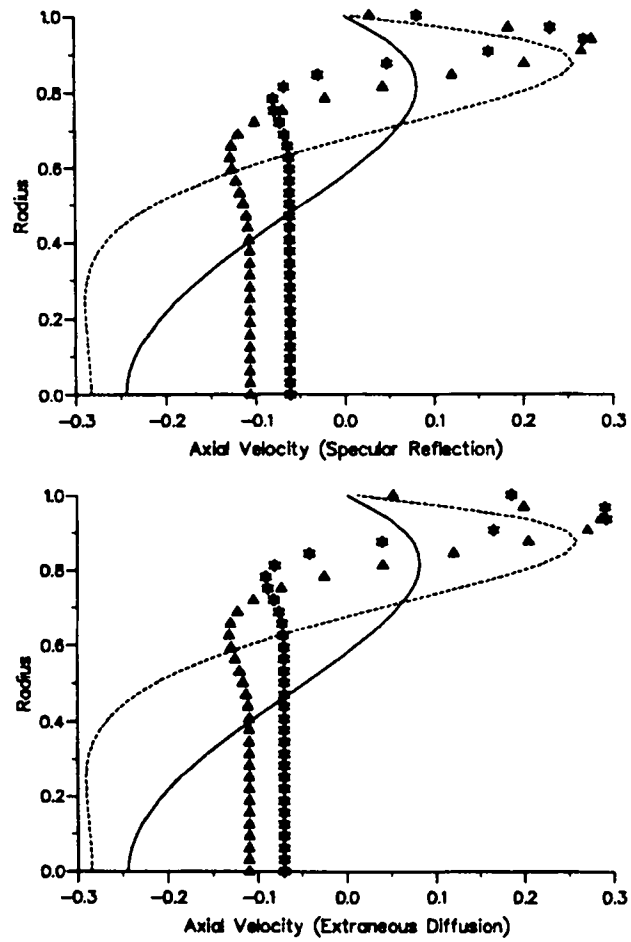

Figure 7. Comparison of developed velocity profiles at various Womersley numbers obtained using extraneous diffusion and specular reflection methods at time $\theta = 2\pi$. Full line denotes $\alpha = 2{\cdot}5$. Broken line denotes $\alpha = 7{\cdot}5$. Triangular markers denote $\alpha = 15{\cdot}0$. Star markers denote $\alpha = 25{\cdot}0$

each piston step. A *KTOL* value of four is used with the specular reflection method to illustrate the increase in axial velocity errors with increasing Womersley number. Numbers of piston positions of 178, 89, 60 and 45 were achieved by varying the value of *NRAT2* from one to four for a mid-range Womersley value of 7·5 and the corresponding increase in overall axial velocity error is shown by Figure 12.

Figure 13 is an example of the downstream axial velocity development at a low Womersley number, $\alpha = 2{\cdot}5$, for the specular reflection method. The plot illustrates the low error in the axial wall velocity, which should be zero, achieved at low Womersley numbers. The singularity at the tube entrance and on the tube wall is clearly seen, as for the Poiseuille flow case, at the maximum reverse piston velocity. The effect of the singularity is not evident at the end of a piston stroke owing to the zero inlet velocity at this time.

The phase difference between the developed centreline velocity obtained using the specular reflection method and that obtained by Womersley[6] for a Womersley number of 3·5 is shown by Figure 14. Initially the Womersley solution lags the present solution by approximately 17°. Figure 14

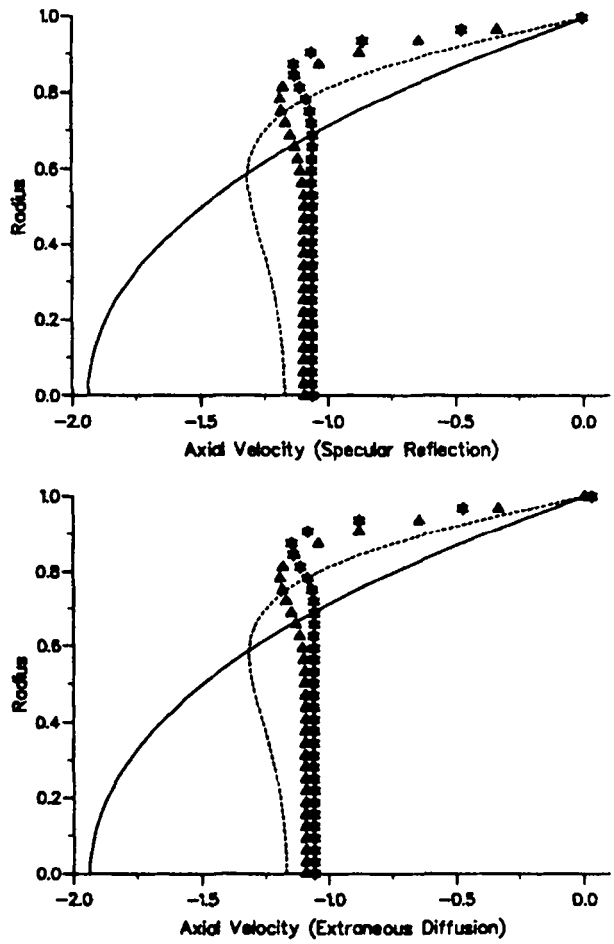

Figure 8. As Figure 7, but at $\theta = 3\pi/2$

shows that the fully developed flow is achieved around approximately 90°, which is one-quarter of the initial sinusoidal piston oscillation. When the developed flow is achieved, both the present and Womersley developed centreline velocities lag the piston velocity by approximately 13°. Figure 15 shows the developed boundary layer thickness and entrance length for a single piston oscillation. The comparison with results obtained using the method of Womersley illustrates the accuracy of the developed boundary layer thickness values. The results obtained analytically by Kassianides and Gerrard[7] for an unsteady low- Womersley-number boundary layer thickness are similar to the present results. The phase difference between the minima of the developed entrance length and boundary layer thickness is approximately 20° on the forward piston motion and approximately 15° on the reverse piston motion, assuming the sinusoidal form of the piston motion defined in Section 6. Figure 15 shows that the maxima of the boundary layer thickness and entrance length are in phase.

Finally, Figure 16 illustrates the CPU time for a single piston oscillation for a range of Womersley numbers employing the extraneous diffusion and specular reflection techniques. The mean ratio of the CPU times for the extraneous diffusion and specular reflection methods is approximately 3·5,

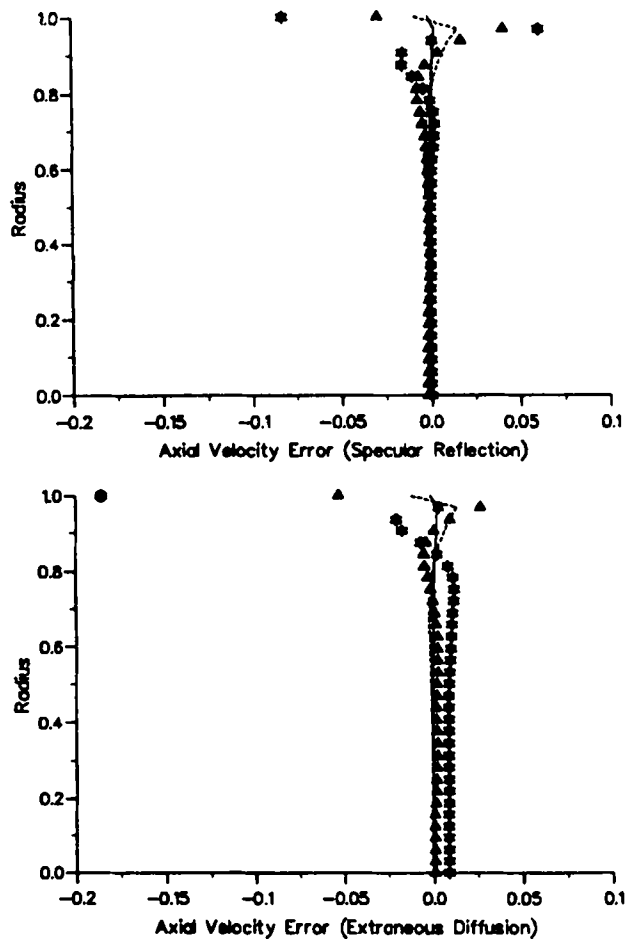

Figure 9. Developed axial velocity errors at various Womersley numbers obtained using extraneous diffusion and specular reflection methods at time $\theta = 2\pi$. Full line denotes $\alpha = 2{\cdot}5$. Broken line denotes $\alpha = 7{\cdot}5$. Triangular markers denote $\alpha = 15{\cdot}0$. Star markers denote $\alpha = 25{\cdot}0$

implying that a significant gain in computing time is achieved when employing the specular reflection method, which displays errors of an order similar to that obtained when using the extraneous diffusion method for oscillating flow.

8. CONCLUSIONS

The adaption of the two-dimensional vorticity transport algorithm of Benson *et al.*[3] to describe steady and oscillating flows in an axisymmetric cylindrical tube has been completed. Errors have been shown to be approximately equal when using both the specular reflection and extraneous diffusion methods and thus, in view of the computing time, the specular reflection method gives sufficient accuracy for most purposes. The method used to describe a developing Poiseuille flow gives accurate developed velocity and vorticity profiles and an accurate estimation of entrance length. The oscillating flow model successfully describes low-Womersley-number flows but gives less accurate solutions at higher Womersley numbers.

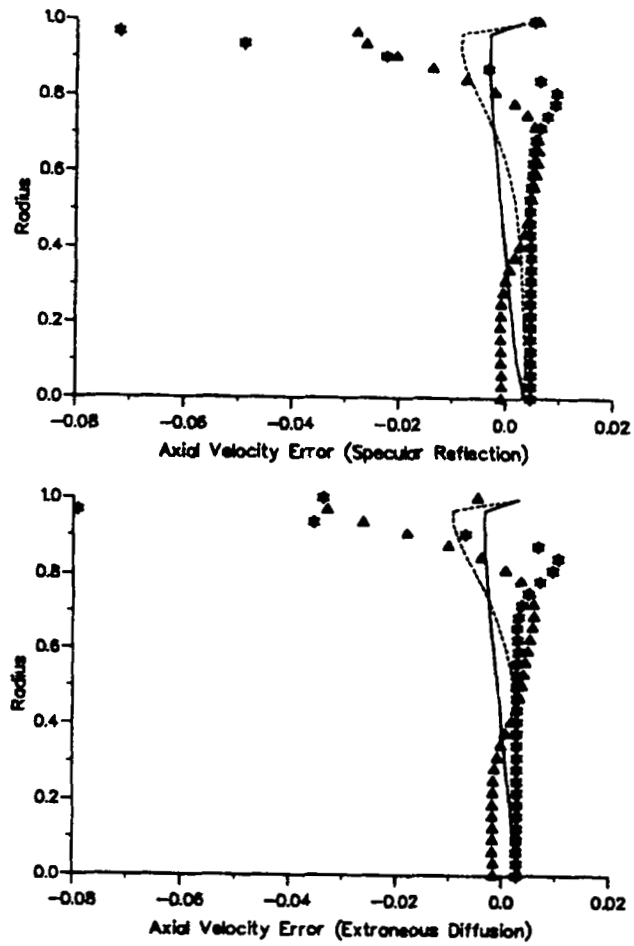

Figure 10. As Figure 9, but at $\theta = 3\pi/2$

In the application of equation (9) in the Appendix to the diffusion of vorticity, the values of the right-hand side of this expression were stored for all the values needed and then extracted when required. Since completing this work, we have realized that a much greater saving could be achieved by an extended use of the symmetry of diffusion and the storage of values. Diffusion from the grid point r_1, z_1 to the points r_2, $z_1 \pm n \cdot DZD$ transfers the same *fraction* of vortex strength as does diffusion from r_1, z_3 to r_1, $z_3 \pm n \cdot DZD$. The fractions separately determined for the whole range of radial points from which vortices diffuse can then be stored. A scan of the mesh in the z-direction then only requires the fraction and strength of the diffusing vortex to determine the whole diffused field. The method can also include diffusion near boundaries and near the centreline.

ACKNOWLEDGEMENTS

This work is supported by the Medical Research Council under grant G 9101792 SA. We gratefully acknowledge the Medical Research Council Research Assistantship held by the first author.

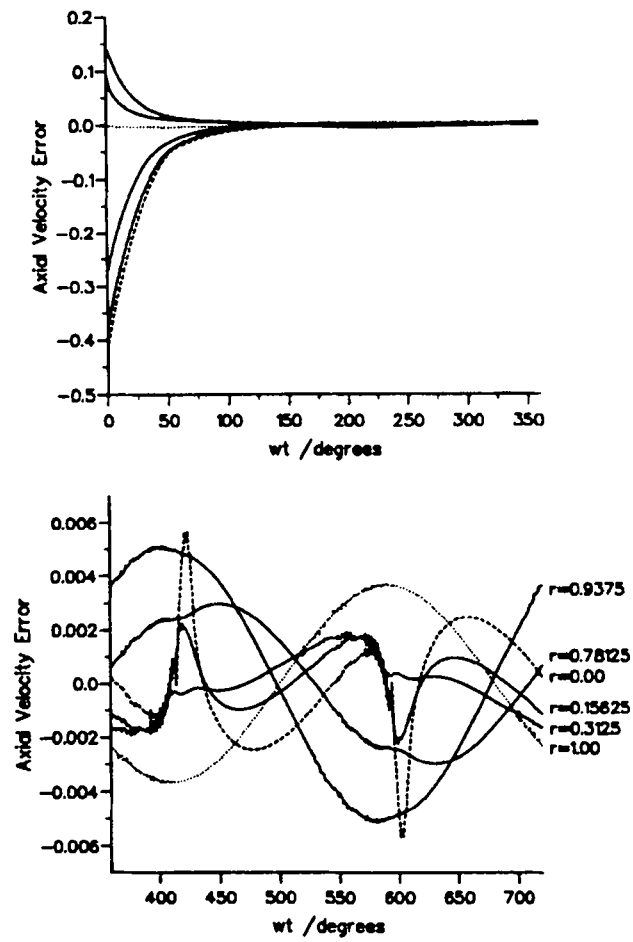

Figure 11. Time development of axial velocity errors at various radii for a Womersley number of 3·5. Dotted line denotes error along wall. Broken line denotes error along centreline

APPENDIX: DIFFUSION OF VORTICITY FOR A VORTEX METHOD COMPUTATIONAL SCHEME IN AXISYMMETRIC FLOWS

In two dimensions the vorticity is everywhere unidirectional and behaves in the same manner as a scalar and in the diffusion process the direction is preserved. In this case the diffusion of heat and of vorticity are governed by equations of the same form with the kinematic viscosity replacing the thermal diffusion coefficient. Diffusion from a straight line source of heat or vorticity produces the Oseen vortex solution. We consider here diffusion from a ring vortex, which is a circular line source of vorticity. In axisymmetric calculations the flow equations can be solved by consideration of a radial plane, but when considering diffusion of vorticity, the whole of the azimuthal plane is important. Vortex elements are vortex rings with their centres on the axis of symmetry. The diffusion of heat for these cases is covered by Carslaw and Jaeger.[13] The adaptation to the diffusion of vorticity can be made provided that one uses the property of axisymmetry, i.e. that the diffusion develops with axisymmetry maintained at all times. When the radius of the ring is very large, diffusion over small distances will be close to the two-dimensional solution. When the radius of the ring is not effectively

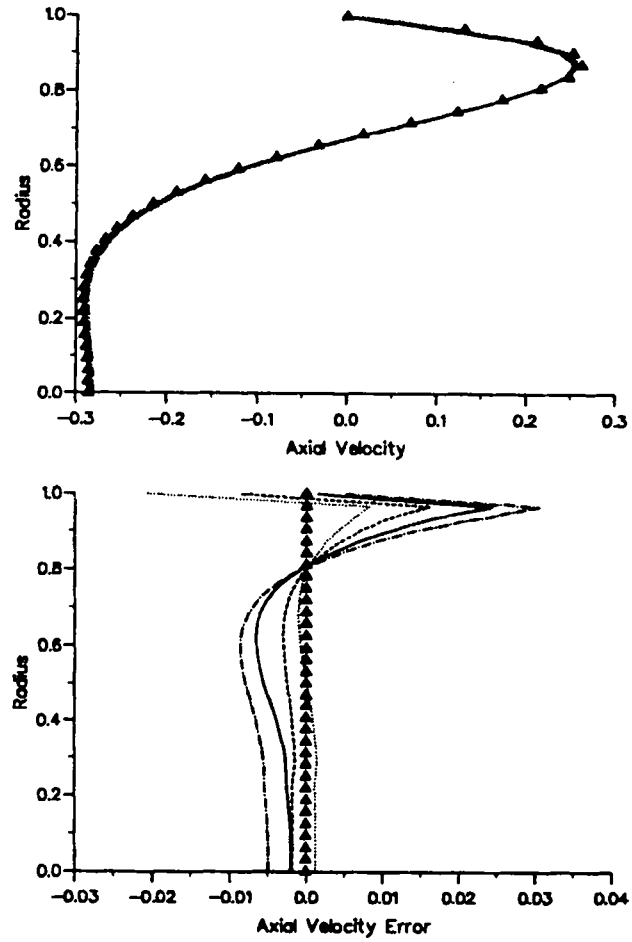

Figure 12. Effect of varying number of piston positions for $\alpha = 7{\cdot}5$. Triangular markers denote exact solution. Chain line denotes $NZP = 45$. Full line denotes $NZP = 60$. Broken line denotes $NZP = 89$. Dotted line denotes $NZP = 178$

infinite, diffusion inwards concentrates the vorticity and diffusion outwards produces an attenuation. Since the areas of cylindrical shells are proportional to the radius, a first approximation to the diffusion from a ring vortex line is the Oseen solution modified by the ratio of the radii. This approximation will be shown to be increasingly inaccurate as the radius diminishes. The exact solution is presented as a correction factor to be applied to the two-dimensional diffusion with a radius ratio correction included.

We are interested only in diffusion from a vortex line and over small distances, because the computing scheme involves only diffusion of zero-age vortices in each (small) diffusion time step. We follow Carslaw and Jaeger,[13] Section 10.3, Case V. They consider instantaneous point sources of heat of strength $Q\mathrm{d}z'$ at a point z'. In the present case this becomes $\Gamma \mathrm{d}z'$, where Γ is the circulation of the vortex ring. Lighthill[14] calls $\Gamma \mathrm{d}z'$ the strength of the vortex element. This determines the scale of

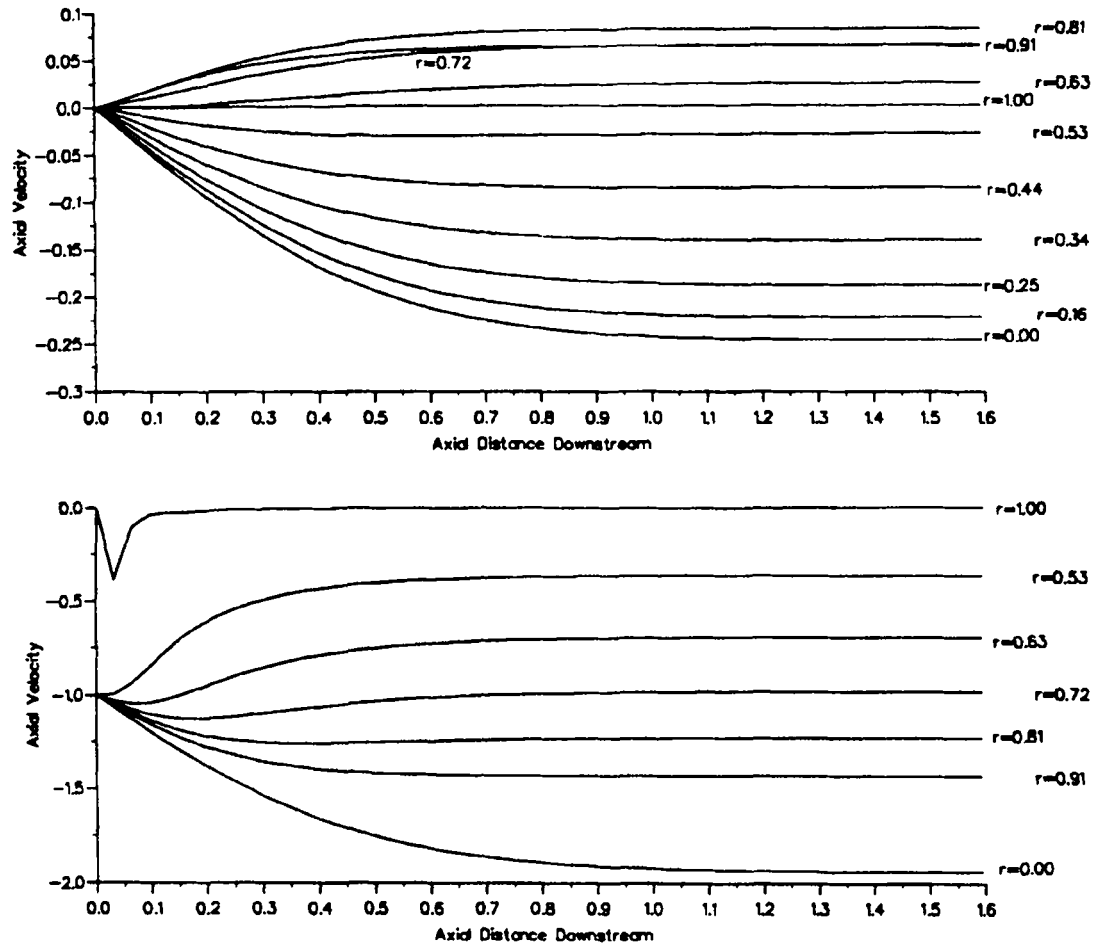

Figure 13. Axial velocity downstream development at various radii at a Womersley number of 2·5 using specular reflection method. Top figure denotes $\theta = 2\pi$. Lower figure denotes $\theta = 3\pi/2$

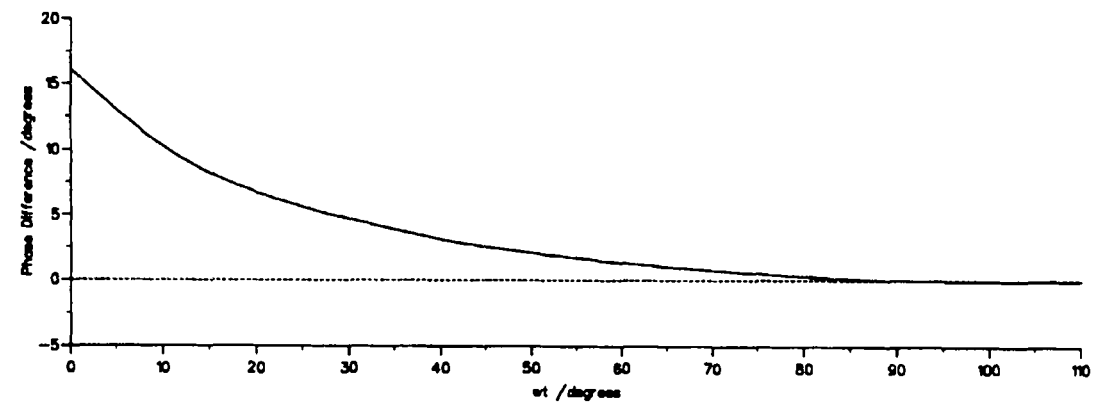

Figure 14. Phase difference between exact and computed centreline velocities at low Womersley number ($\alpha = 3{\cdot}5$). Solid line denotes present results. Broken line denotes exact Womersley solution

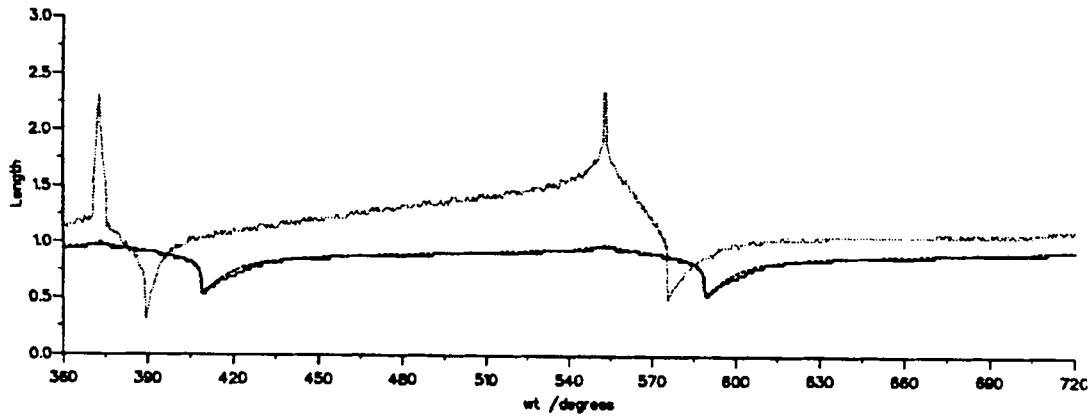

Figure 15. Periodic boundary layer thickness and entrance length at low Womersley number ($\alpha = 3{\cdot}5$). Broken line denotes exact boundary layer thickness. Full line denotes computed boundary layer thickness. Dotted line denotes computed entrance length

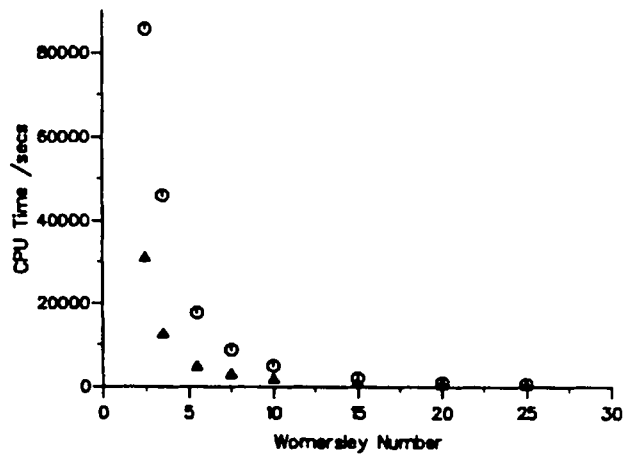

Figure 16. CPU times for a single piston oscillation starting from rest using an HP710 workstation. Triangular markers denote specular reflection. Circular markers denote extraneous diffusion

the velocity field and vorticity is this strength per unit volume. Here the incorporation of the preservation of axisymmetry necessitates alterations. Consider the cross-section shown in Figure 17. Without loss of generality we take the ring to be at $z' = 0$. The vorticity vector is diffused without change in direction. Diffusion from elements S_1 and S_2 must be taken together so that the vector sum of the two diffused vorticities will produce a resultant with no radial component. In this way an extra factor of $2\cos(\theta - \theta')$ is introduced. For convenience we take $\theta = 0$ (whatever the position of the point of observation, P, θ is taken as zero in this direction). The Carslaw and Jaeger integral thus becomes

$$\eta = \frac{\Gamma r'}{9(\pi\nu t)^{3/2}} 2 \int_0^{\pi} e^{-R^2/4\nu t} \cos\theta' \, d\theta', \tag{8}$$

where $R^2 = r^2 + r'^2 + z^2 - 2rr'\cos\theta'$.

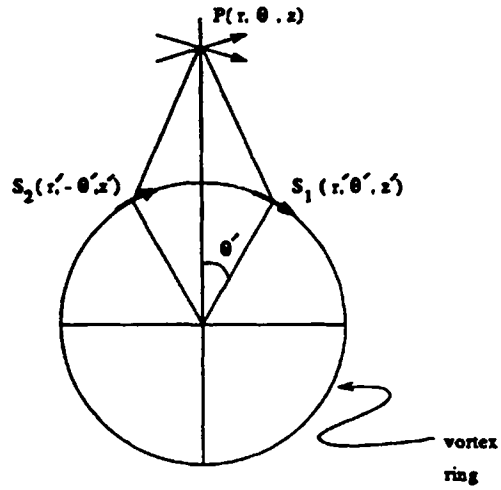

Figure 17. Diffusion of ring vortex in axial plane

With the modified Bessel function of order one given by

$$I_1(x) = \frac{1}{\pi}\int_0^{\pi} e^{x\cos\theta}\cos\theta d\theta$$

equation (8) can be written as

$$\begin{aligned}\eta &= \frac{\Gamma r'}{4(\pi\nu t)^{3/2}} e^{-(r^2+r'^2+z^2)/4\nu t}\int_0^{\pi}\cos\theta' e^{rr'\cos\theta'/2\nu t}d\theta' \\ &= \frac{\Gamma r'}{4(\pi\nu t)^{3/2}} e^{-[(r-r')^2+z^2]/4\nu t} e^{-rr'/2\nu t}\int_0^{\pi} e^{rr'\cos\theta'/2\nu t}\cos\theta' d\theta' \\ &= \frac{\Gamma}{4\pi^{1/2}\nu t}\frac{r'}{(\nu t)^{1/2}} e^{-R_{\min}^2/4\nu t} e^{rr'/2\nu t} I_1\left(\frac{rr'}{2\nu t}\right),\end{aligned}$$

where $R_{\min}$ is the minimum distance of P from the vortex ring at $\theta = \theta' = 0$; see Figure 18. $R_{\min}$ is the distance in the radial plane within which the axisymmetric solution is obtained. Finally,

$$\frac{\eta}{\eta_{os}} = \pi^{1/2}\frac{r}{(\nu t)^{1/2}} e^{-rr'/2\nu t} I_1\left(\frac{rr'}{2\nu t}\right), \tag{9}$$

where η_{os} is the Oseen diffusion multiplied by the radius ratio r'/r.

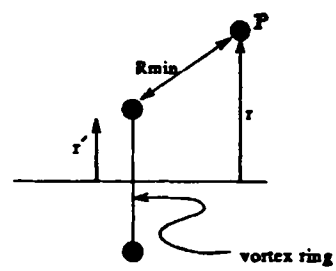

Figure 18. Diffusion of ring vortex in azimuthal plane

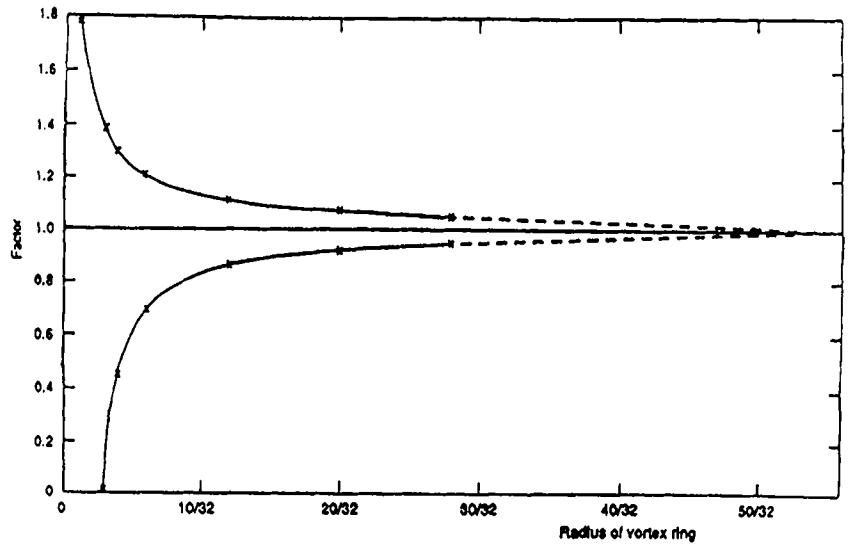

Figure 19. Factor on, ζ_{oseen} with radius ratio, to give correct diffusion. Diffusion 3/32 of ring radius inwards and outwards for $Re_d = 40$

The series to be summed to give $I_i(x)$ and $e^{-x}I_1(x)$ can be found in Reference 15 and the values obtained are incorporated in the computing scheme to determine the correction factors of equation (9). A particular case is plotted in Figure 19, which shows the value of equation (9) for a vortex of varying diameter in a tube of radius unity and a cross-sectional mean velocity of unity. The Reynolds number based on diameter is 40 with $\nu = 0{\cdot}05$ and the diffusion time step t is 0·00972. Distance steps are 1/32 and diffusion is over three distance steps in one time step. The figure shows the significant difference between axisymmetric and two-dimensional diffusion. The difference decreases with increasing radius, but only at large r is the difference small. When diffusion takes place from a ring vortex on a mesh point to other mesh points, a table of all the values of equation (9) which will be needed can be stored initially and abstracted when required.

REFERENCES

1. A. Leonard, 'Computing three-dimensional incompressible flows with vortex elements', *Ann. Rev. Fluid Mech.*, **17**, 523–559 (1985).
2. K. Chua and T. R. Quackenbush, 'Fast three-dimensional vortex method for unsteady wake calculations', *AIAA J.*, **31**, 1957–1958 (1993).
3. M. G. Benson, P. G. Bellamy-Knights, J. H. Gerrard and I. Gladwell, 'A viscous splitting algorithm applied to low Reynolds number flows round a circular cylinder', *J. Fluids Struct.*, **3**, 439–479 (1989).
4. J. P. Christiansen, 'Numerical simulation of hydrodynamics by the method of point vortices', *J. Comput. Phys.*, **13**, 363–379 (1973).
5. M. H. Wagner, 'Developing flow in circular conduits: transition from plug flow to tube flow', *J. Fluid Mech.*, **72**, 257–268 (1975).
6. J. R. Womersley, 'Oscillatory motion of a viscous liquid in a thin walled elastic tube', *Philos. Mag.*, **46**, 199–221 (1955).
7. E. Kassianides and J. H. Gerrard, 'The calculation of entrance length in physiological flow', *Med. Biol. Eng.*, **13**, 558–560 (1975).
8. M. Friedmann, J. Gillis and N. Liron, 'Laminar flow in a pipe at low and moderate Reynols numbers', *Appl. Sci. Res.*, **19**, 426–438 (1968).
9. H. Schlichting, *Boundary Layer Theory*, Pergamon, Oxford, 1955.
10. A. J. Chorin, 'Numerical study of slightly viscous flow', *J. Fluid Mech.*, **57**, 785–796 (1973).

11. L. H. Benson and S. A. Trogden, 'An eigenvalue solution of entry flow in a semi-infinite pipe at low Reynolds numbers', *Appl. Sci. Res.*, **42**, 347–359.
12. H. B. Atabek, C. C. Chang and L. M. Fingerson, 'Measurement of laminar oscillatory flow in the inlet length of a circular tube', *Phys. Med. Biol.*, **9**, 219–227 (1964).
13. H. S. Carslaw and J. C. Jaeger, *Conduction of Heat in Solids*, 2nd edn, Clarendon, Oxford, 1959.
14. M. J. Lighthill, 'The image system of a vortex element in a rigid sphere', *Proc. Camb. Philos. Soc.*, **52**, 317–321 (1956).
15. M. Abramowitz and I. A. Stegun (eds), *Handbook of Mathematical Functions*, Dover, New York, 1968.